SCIENTIFIC REPORTS

OPEN

# Heat-induced Bone Diagenesis Probed by Vibrational Spectroscopy

M. P. M. Marques[1,2], A. P. Mamede[1], A. R. Vassalo[1,3,4], C. Makhoul[1,3], E. Cunha[2,3], D. Gonçalves[3,4,5], S. F. Parker[6] & L. A. E. Batista de Carvalho[1]

Received: 21 August 2018
Accepted: 12 October 2018
Published online: 29 October 2018

**Complementary vibrational spectroscopic techniques – infrared, Raman and inelastic neutron scattering (INS) – were applied to the study of human bone burned under controlled conditions (400 to 1000 °C). This is an innovative way of tackling bone diagenesis upon burning, aiming at a quantitative evaluation of heat-induced dimensional changes allowing a reliable estimation of pre-burning skeletal dimensions. INS results allowed the concomitant observation of the hydroxyl libration ($OH_{libration}$), hydroxyl stretching ($\nu$(OH)) and ($OH_{libration} + \nu$(OH)) combination modes, leading to an unambiguous assignment of these INS features to bioapatite and confirming hydroxylation of bone's inorganic matrix. The $OH_{lib}$, $\nu$(OH) and $\nu_4(PO_4^{3-})$ bands were identified as spectral biomarkers, which displayed clear quantitative relationships with temperature revealing heat-induced changes in bone's H-bonding pattern during the burning process. These results will enable the routine use of FTIR-ATR (Fourier Transform Infrared-Attenuated Total Reflectance) for the analysis of burned skeletal remains, which will be of the utmost significance in forensic, bioanthropological and archaeological contexts.**

Bone is a biphasic material comprising a protein component (mostly collagen I) within an inorganic matrix of hydroxyapatite ($Ca_{10}(PO_4)_6OH_x$, HAp), the hydroxyl and phosphate groups being partly substituted by carbonate (respectively A- and B-type carbonates)[1,2]. Upon diagenesis – *post-mortem* processes triggering physical and chemical alterations – bone undergoes changes in molecular structure, namely recrystallisation (associated with collagen loss) leading to an increase in crystal size, carbonate depletion and uptake of anions from the environment (*e.g.* fluoride)[3–11].

Human bones are often found in both archaeological and forensic contexts, and their importance for the study of past populations or for victim identification in forensic investigations is unquestionable (*e.g.* 9/11 terrorist attacks, 2009 Victoria bush fires). The examination of human skeletal remains may allow to establish biological profiles and thus contribute to the positive identification of the deceased. Also, it helps with inferring about the circumstances of death. However, bone vestiges can be found in diverse conditions and it is not unusual that the body has been subject to heat, upon events such as cremation, aircraft accidents, bush fires or acts of terrorism. In this case, to retrieve reliable information from the analysis of bones carries a high degree of uncertainty, because heat renders hydroxyapatite more accommodating to substitutions and often induces significant changes to the skeleton, which interferes with the reliability of the available osteometric methods[9,11–17]. Indeed, the techniques commonly used for human identification from burned bones and teeth are conceived for unmodified dimensions, while burning at high temperatures leads to considerable changes in the form of shrinkage or (more rarely) expansion. Overcoming this obstacle has been hindered by a scarcity of research on burned human remains, often for lack of accessible skeletons. This has had major implications, preventing anthropologists from being able to generate unequivocal biological profiles of both modern-day victims and individuals from past populations whose remains were recovered from archaeological settings.

Diagenesis-induced chemical alterations in bone (*e.g.* fluoridation, carbonate substitution or mineral uptake) can be accurately detected by optical vibrational spectroscopy (infrared and Raman). Additionally, Raman is the tool of choice for determining the presence of organic components, mainly collagen[18], and has recently been used successfully for sub-surface probing of bone samples (through Spatially-Offset Raman spectroscopy (SORS))[19].

[1]Molecular Physical Chemistry R&D Unit, Department of Chemistry, University of Coimbra, Coimbra, Portugal. [2]Department of Life Sciences, University of Coimbra, Coimbra, Portugal. [3]Laboratory. Forensic Anthropology, Centre for Functional Ecology, University of Coimbra, Coimbra, Portugal. [4]Research Centre for Anthropology and Health (CIAS), University of Coimbra, Coimbra, Portugal. [5]Archaeosciences Laboratory., Directorate General Cultural Heritage (LARC/CIBIO/InBIO), Lisbon, Portugal. [6]ISIS Facility, STFC Rutherford Appleton Laboratory, Chilton, Didcot, OX, 11 0QX, United Kingdom. Correspondence and requests for materials should be addressed to L.A.E.B.d.C. (email: labc@ci.uc.pt)

However, the marked fluorescence of bone (mainly assigned to its organic constituents) may limit the observation of the Raman signal[20], particularly when the samples were not subject to high temperatures (>600 °C). Although this may be partially overcome by the use of near-infrared excitation (Fourier transform Raman, with a 1064 nm laser), Fourier transform infrared spectroscopy (FTIR) is nowadays the most commonly applied vibrational spectroscopic technique for these kinds of studies. A clear increase in recent years has been observed in its application within the forensic[15] and archaeological[21–24] sciences. For example, its potential for discriminating between fossilised, archaeological and modern bones[24–26] or for estimating the postmortem interval in forensic cases[27–30], has been demonstrated by evaluating bone crystallinity, as well as carbonate and organic contents. Nonetheless, devising a method capable of quantifying diagenetic changes in burned skeletal remains is still an unmet challenge. Although previous studies have attempted to tackle this issue by infrared spectroscopy[4,5,9–11,31–35], an approach based on the intrinsic properties of bone (microcrystalline structure) was firstly followed by the authors through the application of inelastic neutron scattering (INS) spectroscopy to human bones burned under controlled conditions[36].

The present study comes as a continuation of these promising results, using complementary vibrational spectroscopy techniques (both optical and neutron-based) with a view to attain, in the near future, a method that will enable us to extract quantitative information from burned human bones and estimate pre-burning skeletal dimensions in a reliable and consistent way. The main premise of that work is that the measured dimensional changes are primarily due to variations in the crystal structure of bioapatite, as heating is known to lead to an increased crystallite size and a decreased lattice strain (*i.e.* higher organisation). This is reflected in the crystallinity index (CI) and other spectroscopic ratios mainly obtained from infrared data[4,5,10,11], which can then be used to assess the conditions of the burning process (*e.g.* temperature and duration) that affected the bones. Hence, a correlation will be sought between the pre-burning bone dimensions and the experimental set of data obtained for the burned samples: macroscopic heat-induced dimensional changes, and relevant spectroscopic biomarkers and indexes. The fact that variations in the elemental structure of bone are clearly reflected in its vibrational fingerprint fully justifies the use of vibrational spectroscopic methods to monitor bone diagenesis upon burning. Unlike optical techniques – Raman and FTIR[6,8–11,24,32,37,38] – only a limited number of INS studies of bone have been carried out successfully in the last decade[36,39–41]. Nevertheless, these allowed detection of distinctive features such as changes in carbonate and water content, chemical substitutions at the hydroxyl sites and heat-elicited variations, revealing even minor differences in bone composition and being able to relate these to external factors affecting the skeletal samples (burning and/or other environmental events). INS is an extremely useful technique for probing a hydrogenous material such as bone, the intensity of each vibrational transition being expressed, for a given atom, by the dynamic structure factor

$$\mathbf{S_i^*(Q,\ \nu_k)} = \frac{(\mathbf{Q^2 u_i^2})\sigma}{\mathbf{3}}\mathbf{exp}\left(-\frac{\mathbf{Q^2\alpha_i^2}}{\mathbf{3}}\right) \quad (1)$$

where $Q$ (Å$^{-1}$) is the momentum transferred to the sample, $\nu_k$ is the energy of a vibrational mode, $u_i$(Å) is the displacement vector of atom $i$ in mode $k$, $\sigma$ is the neutron scattering cross section of the atom, and $\alpha_i$(Å) is related to a mass-weighted sum of the displacements of the atom in all vibrational modes. There are no selection rules for INS (in contrast to FTIR and Raman) which yields all the fundamental modes, overtones and combination bands for the analysed samples.

Complementary INS, Raman and FTIR (in attenuated total reflection mode, ATR) were applied to samples of human bone burned under controlled conditions (from 400 to 1000 °C). This is an innovative way of probing human bone tissue that will provide an improved understanding of heat-induced diagenesis and will lead to a quantitative method for assessing the associated structural and dimensional changes.

## Results and Discussion

The human skeletal remains currently analysed were burned under controlled laboratory conditions, at different temperatures (from 400 to 1000 °C). The process of bone combustion (burning under aerobic conditions) comprises several stages (Fig. 1)[12,42]: (i) dehydration – breakage of hydroxyl bonds and water removal (water molecules adhering to the hydroxyapatite crystals and bound to the organic constituents); (ii) decomposition of the organic components (lipids and proteins, at *ca.* 400 to 550 °C); (iii) inversion – carbonate loss upon heating (disappearing completely at *ca.* 700 °C); (iv) fusion (at >700 °C) – changes in crystallinity usually accompanied by an increase in crystal size, and $OH^-$ and $PO_4^{3-}$ rearrangement within the pores left by the water and organic components. This thermal decomposition may be affected by the organic content of the bone, that acts as a shield against thermal damage protecting the inorganic component and thus leading to a delayed alteration of this mineral phase[43]. Thus, it is not until quite high temperatures are attained that the bone's inorganic component is affected, microcrystallinity alterations taking place only above 700 °C. Actually, this temperature was found to be borderline, the most significant spectral changes having been detected above it (both by FTIR and INS), as discussed below.

In the present work, the application of complementary vibrational spectroscopic techniques (optical and neutron-based) delivered the whole vibrational profile of the bone samples under analysis: (i) the main bands ascribed to phosphate ($PO_4^{3-}$) and carbonate ($CO_3^{2-}$) groups, as well as to bone's organic constituents (amide signals/proteins and $CH_2$ deformation and stretching modes/lipids), obtained by Raman and FTIR; (ii) bioapatite's OH librational and stretching bands, clearly detected by INS[36] but not always seen in the optical spectra; (iii) the characteristic modes of the crystal lattice, associated with the short-range order and hydrogen-bonding profile within the crystalline framework (therefore reflecting bone's heat-induced dimensional changes), that can only be accessed by neutron spectroscopy. Furthermore, the use of the MAPS and TOSCA INS spectrometers enabled the

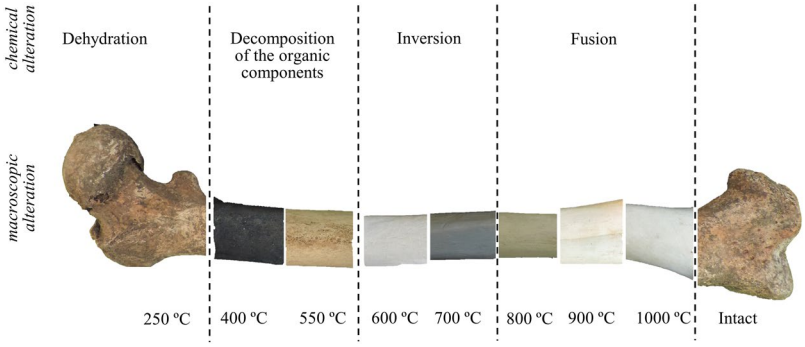


**Figure 1.** Schematic representation of the several stages of bone combustion.

observation, with very high sensitivity, of both the low frequency region (<1000 $cm^{-1}$, in TOSCA) and the high wavenumber range (in MAPS). Additionally, MAPS allowed the simultaneous detection of the OH librational and stretching signals from bioapatite.

**Infrared and Raman Spectroscopy.** For the currently studied samples, infrared data was measured in reflectance mode (FTIR-ATR), covering a wide spectral window from the far- to the mid-IR (50 to 4000 $cm^{-1}$), which has been shown to be a rapid, easy and cost-efficient method providing very reliable and reproducible results on bone, without any particular sample preparation and in a completely non-destructive way. In addition, these measurements have shown a higher reproducibility as compared to transmission FTIR (involving manual pellet creation) and other infrared methodologies such as diffuse reflectance infrared Fourier transform spectroscopy (DRIFTS, requiring sample mixing with KBr without pelleting)[8].

Although the high fluorescence of bone, that restricts the observation of its Raman spectrum, can be slightly decreased by cleaning the bone fragments prior to measurement[44], these are rather invasive procedures that were not applied in this work due to their potential interference in the bone's characteristics, which we aimed to determine solely as a function of the heating temperature (for a constant burning time). Therefore, reliable Raman data was only obtained for bones subject to temperatures above 600 °C that yielded clearly observable bands.

Table 1 comprises the complete vibrational data (infrared, Raman and INS) measured for the human bones presently analysed and the corresponding assignments – both the high (>700 °C) and low temperature (<700 °C) vibrational signatures.

Figure 2 contains the FTIR-ATR spectra of human humeri, unburned and burned at defined temperatures from 400 to 1000 °C, as well as the infrared profile of reference hydroxyapatite (HAp). For the samples subject to temperatures below 700 °C, the infrared signature of bone's organic constituents was clearly detected: from the lipids – a broad $CH_2$ deformation band centred at 1450 $cm^{-1}$ and a CH stretching feature at *ca.* 2950 $cm^{-1}$ – and from the protein (mainly collagen type I) – amide I (1660 $cm^{-1}$), amide II (1550 $cm^{-1}$) and amide III (1250 $cm^{-1}$). This organic matrix was completely destroyed above 700 °C, the lipidic constituents being the first to be removed, yielding a vibrational pattern very similar to the one formerly obtained for the same bone samples after defatting/deproteination procedures[45].

The trigonal planar carbonate ions within bone yield distinctive signals at 1415/1460 $cm^{-1}$ ($\nu_3(CO_3^{2-})$). The band from $\nu_3(PO_4^{3-})$ dominates the spectra, at 1025 $cm^{-1}$, surrounded by the features assigned to $\nu_1(PO_4^{3-})$ (960 $cm^{-1}$) and $\nu_3(PO_4^{3-})$ from a second phosphate site (at 1087 $cm^{-1}$, probably due to the presence of fluorapatite (francolite)), the latter being gradually obscured by the broadening of the $\nu_3^{as}(PO_4^{3-})$ signal at temperatures below 600 °C. In addition, a shoulder is detected at *ca.* 983 $cm^{-1}$ for the samples burned at 900 and 1000 °C, assigned to $\nu_1(HPO_4^{2-})$. The lower frequency range comprises the features ascribed to $\nu_4(PO_4^{3-})$ (565 and 605 $cm^{-1}$) and $\nu_2(PO_4^{3-})/\nu_2(HPO_4^{2-})$ (*ca.* 470 $cm^{-1}$), as well as $\nu$(Ca–OH) (*ca.* 330 and 230 $cm^{-1}$), $OH_{translation}$ (at *ca.* 340 $cm^{-1}$) and (Ca–$PO_4$) lattice modes (below 300 $cm^{-1}$) from bone's inorganic framework. The heat-induced reorganisation of bioapatite's microcrystalline structure is revealed by the progressive narrowing of the bands upon increasing temperatures, coupled to the appearance of the characteristic signals from the hydroxyl groups at temperatures above 700 °C – $(OH)_{libration}$ and $(OH)_{stretch}$ at 630 and 3570 $cm^{-1}$, respectively.

The vibrational profile currently observed for the bone carbonates deserves particular attention: the main detected features (at *ca.* 1415/1450/1460 $cm^{-1}$) are ascribed to the $\nu_3(CO_3^{2-})$ asymmetric stretching (Table 1, Fig. 2), its threefold splitting being suggested to be due to the two distinct types of carbonate present in bioapatite. These display different orientations within the lattice, either perpendicular (type A) or parallel (type B) to the *c* axis, corresponding, respectively, to a $CO_3^{2-}$ substitution of either $OH^-$ (in the channels) or $PO_4^{3-}$ (in the tetrahedral sites) within the apatitic structure[46–49]. These features undergo a marked decrease upon heating (>700 °C, Fig. 2), being almost absent in the samples burned at 1000 °C, as previously verified for carbonate apatites[49], which is consistent with carbonate loss upon bone heating. This behaviour of the $\nu_3(CO_3^{2-})$ modes is in agreement with other reported work on the temperature dependence of the carbonate content of both mineral and skeletal samples. Owing to their distinct structures, carbonates A and B have been reported to display different thermal decomposition mechanisms, as they occupy sites within the inorganic network which are not equally affected by high temperatures[48,49]. Also, for synthetic calcium carbonate minerals it was found that $\nu_3(CO_3^{2-})_B$ is more responsive to external changes[50] (such as heating), mainly due to structural differences within the bioapatite

| <700 °C | | | >700 °C | | |
|---|---|---|---|---|---|
| FTIR-ATR | INS | Assignment | FTIR-ATR | Raman | INS |
| | | $OH_{lib} + OH_{stretching}$ | | | 4250 |
| | | $OH_{stretching}$ | 3570 | 3570 | 3570 |
| 3300 | 3385 | $OH_{water\ stretching}$ | | | |
| 2960–2850 | 2974 | $CH_{stretching}$ | | | |
| | 2560 | 3rd overtone $OH_{libration}$ | | | 2560 |
| | 1941 | 2nd overtone $OH_{libration}$ | | | 1941 |
| 1660 | 1660 | amide I | | | |
| 1650 | 1650 | $(H_2O)_{deformation}$ | | | |
| 1550 | 1550 | amide II | | | |
| 1450 | 1450 | $(CH_2)_{deformation}$ | | | |
| 1460–1415 | | $\nu_3(CO_3^{2-})$ | 1460–1415 | | |
| | 1302 | 1st overtone $OH_{libration}$ | | | 1302 |
| 1250 *w* | 1250 | amide III | | | |
| | | $\nu_1(CO_3^{2-})_B$ | | 1076 | |
| | | $\nu_3(PO_4^{3-})_{fluorapatite}$ | 1087 | 1028–1054 | |
| 1025 | | $\nu_3(PO_4^{3-})$ | 1025 | | |
| | | $\nu_1(HPO_4^{2-})$ | 983 *sh* | | |
| 960 | | $\nu_1(PO_4^{3-})$ | 960 | 960 | |
| 700 *w* | | $\nu_4(CO_3^{2-})$ | 700 *w* | | |
| 630 | 650 | $OH_{libration}$ | 630 | | 638, 657 |
| 565, 605 | | $\nu_4(PO_4^{3-})$ | 565, 605 | 578–617 | 574–617 |
| 470 | | $\nu_2(PO_4^{3-})/\nu_2(HPO_4^{2-})$ | 470 | 429–446 | 450 |
| | | $OH_{translation}$ | 340 | 335 | 330–350 |
| | | $\nu(Ca–OH)_{lattice}$ | 330, 230 *sh* | 329 | 330–350 |
| | 250 | $(CH_3)_{torsion}$ | | | |
| | | $\nu(Ca–PO_4)_{lattice}$ | 170, 210, 265 | 150, 200, 280 | 150, 190, 280 |
| | | $\nu(Ca–PO_4)_{lattice,\ translation}$ | 85 | 138 | 70, 100 |

**Table 1.** Experimental (INS, FTIR and Raman) vibrational wavenumbers ($cm^{-1}$) for the human bones analysed in this study (powdered samples), subject to different burning temperatures (in aerobic conditions)[a]. *sh* – shoulder; *w* – weak.

matrix (*e.g.* planar *vs* non-planar arrangements of the $CO_3^{2-}$ units). The bands currently observed at 1415 and 1460 $cm^{-1}$ are ascribed to type B carbonates and were shown to be more prone to heat-induced removal, their intensity decreasing faster with increasing temperatures as compared to the signal at 1450 $cm^{-1}$ assigned to carbonates A and B.

The complementary Raman results obtained for the bone samples presently studied (subject to temperatures above 700 °C) allowed access to vibrational modes not clearly detected by FTIR (Table 1, Fig. 3): (i) ($Ca–CO_3$) lattice vibrations (*ca.* 140–280 $cm^{-1}$), that did not show a particularly strong temperature dependence; (ii) phosphate modes – $\nu_2(PO_4^{3-})$ at 429/446 $cm^{-1}$, $\nu_4(PO_4^{3-})$ from 578 to 617 $cm^{-1}$, $\nu_1(PO_4^{3-})$ dominating the spectra at 960 $cm^{-1}$, and $\nu_3(PO_4^{3-})$ at 1028–1054 $cm^{-1}$; (iii) and a characteristic carbonate band at 1076 ($\nu_1(CO_3^{2-})_B$) (not observed in the infrared profile since it is obscured by the very intense $\nu_3^{as}(PO_4^{3-})$ signal at 1025 $cm^{-1}$). The broadening of the phosphate symmetric stretching ($\nu_1(PO_4^{3-})$) for decreasing temperatures (900 to 700 °C) reflects a higher disorder of the bioapatite lattice, associated with a larger amount of $CO_3^{2-}$ ions (substituting either $OH^-$ or $PO_4^{3-}$), since Raman spectroscopy is very sensitive to the short-range order within a unit cell. In addition, it should be emphasized that this variation in the bone's carbonate content is closely related to alterations in the growth morphology and crystallite size, that are known to take place upon temperature changes – a higher atomic disorder corresponding to smaller crystal dimensions (in the nanometre scale), the lattice becoming progressively more ordered with increasing temperatures (upon $CO_3^{2-}$ loss).

**INS.** High quality INS spectra were obtained for the burned samples, as they were free from the features assigned to the bone's organic matrix (due to the protons from water, lipids and collagen)[51], which were progressively destroyed by the burning process. This ensured a clear detection of the signals from hydroxyapatite, particularly the OH libration (centred at 650 $cm^{-1}$), which reflects the H-bonding network within bone's inorganic lattice. Interpretation of the data was assisted by previous results obtained for non-burned bovine and rat bones[39,40] as well as by the first reported INS results on burned human bones[36].

Special attention was paid to the bioapatite's OH vibrational modes, prone to undergo marked changes upon heat-induced variations in the crystalline framework. For the samples subjected to very high temperatures (>800 °C) measured in MAPS, the OH libration and stretching signals were detected simultaneously (respectively at *ca.* 650 and 3570 $cm^{-1}$) as well as the ($OH_{libration} + OH_{stretch}$) combination band (at *ca.* 4250 $cm^{-1}$) and the first,

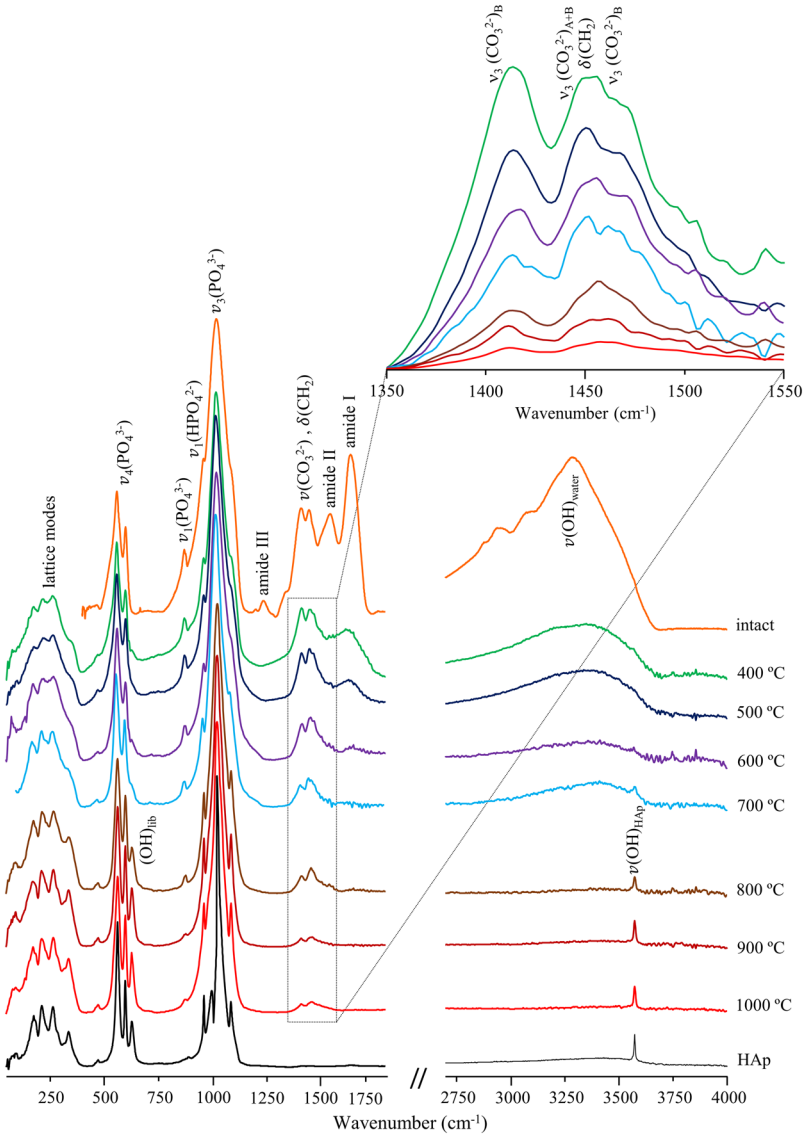


**Figure 2.** FTIR-ATR spectra (far- and mid-IR regions) of human humerus: intact and burned at different temperatures (400 to 1000 °C). The insert shows a magnification of the asymmetric stretching carbonate bands ($\nu_3(CO_3^{2-})$). The spectrum of reference calcium hydroxyapatite (HAp, SRM 2910b) is also shown for comparison.

second and third overtones of the hydroxyl libration (at 1302, 1941 and 2560 cm$^{-1}$) (Fig. 4). This concomitant observation of $OH_{stretch}$ and $(OH_{libration} + OH_{stretch})_{comb}$ allowed an irrefutable assignment of these INS features to bioapatite. Hence, bioapatite's hydroxylation was definitely confirmed by these results (that corroborate those previously reported by the authors)[36].

For the unburned bones, the spectra were dominated, as expected, by features from lipids and protein (mostly collagen I) at *ca*. 250 (protein methyl torsion), 1250 (amide III), 1450 ($CH_2$ deformation), 1550 (amide II), 1660 (amide I) and 2974 cm$^{-1}$ (CH stretching). These gradually disappeared upon heating: the lipidic components at *ca*. 500 °C, followed by the proteins that are hardly noticeable at 700 °C and completely destroyed at 900 °C. The main signals from the hydroxyapatite matrix were thus unveiled at temperatures above 700 °C (Figs 4 and 5).

An increased degree of crystallinity for higher burning temperatures (as previously reported)[40] was evidenced by the noticeable narrowing of the INS signals, mainly the $OH_{libration}$ band at 650 cm$^{-1}$. Crystallinity reached a maximum at 900 °C, the corresponding spectral profile displaying a remarkable resemblance to that of the highly crystalline hydroxyapatite reference (SRM 2910b from NIST) (Figs 4 and 5).

The data recorded in TOSCA allowed access to the low energy range of the spectrum with very high sensitivity (Fig. 5), yielding relevant information on specific vibrational features particularly informative of the type of organization within the solid matrix[7,52]: (i) $Ca^{2+}$ and $PO_4^{3-}$ sublattice translational and $PO_4^{3-}$ librational modes (below 300 cm$^{-1}$), extremely sensitive to crystallinity and evidencing changes mainly between 700 and 800 °C; (ii) (Ca–OH) stretching and OH translation from hydroxyapatite (330–350 cm$^{-1}$); (iii) $\nu_2(HPO_4^{2-})$ and $\nu_2(PO_4^{3-})$ (*ca*. 450 cm$^{-1}$), the former being very difficult to detect by optical vibrational techniques; (iv) $\nu_4(PO_4^{3-})$

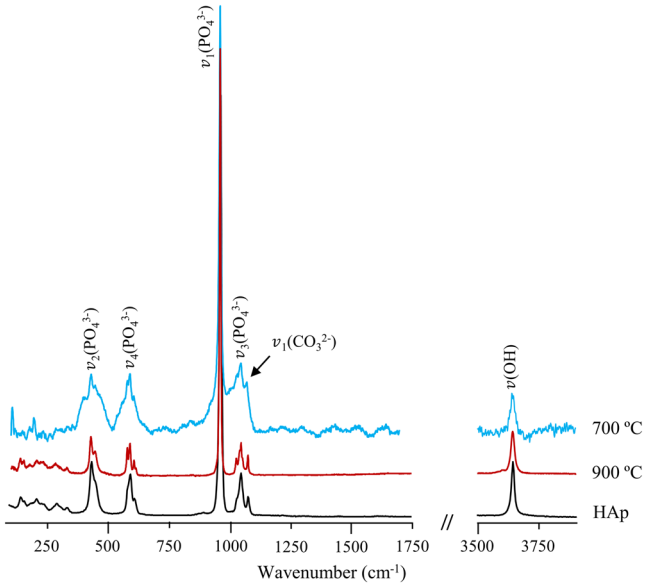


**Figure 3.** Raman spectra of human femur, burned at 700 and 900 °C. The spectrum of reference calcium hydroxyapatite (HAp, SRM 2910b) is also shown for comparison.

(574–617 cm$^{-1}$), suggested to be due to distinct hydroxyapatite polymorphic species (hexagonal and monoclinic forms displaying very subtle and temperature-dependent structural differences); (v) splitting of the hydroxyapatite's OH librational band (at 650 cm$^{-1}$) due to the corresponding in-phase and out-of-phase modes (indistinguishable below 600 °C); (vi) $CH_3$ torsion (at *ca.* 250 cm$^{-1}$), detected for unburned bones due to the presence of protein. In particular, the $\nu_3$(Ca–OH) mode at 330 cm$^{-1}$ was observed only for burning temperatures equal or above 700 °C, being absent for the lower temperatures (Fig. 5(B)), which is justified by the expected $CO_3^{2-}$ by OH substitution within the bioapatite network with increasing temperature (Table 2). In turn, the (Ca–$CO_3^{2-}$) vibrations (typically around 150 and 280 cm$^{-1}$) were not clearly distinguishable below 700 °C, since they were hidden by the (Ca–$PO_4$) lattice modes.

A noticeable temperature dependence was found for several INS features detected for the samples under study: (i) for the lowest energy $\nu_4(PO_4^{3-})$ signal (Fig. 6(A)), its frequency decreasing (by up to *ca.* 6 cm$^{-1}$) for lower temperatures, until it becomes indistinguishable below 600 °C; (ii) for bioapatite's OH librational and stretching signals, that are progressively separated as temperature increases (the former shifting to lower frequencies while the latter deviates to the blue) (Fig. 6(B–D)). These quantitative relationships between particular spectral bands and heating temperature are clear evidence of rearrangements in the hydrogen-bond pattern within the hydroxyapatite network, concurrent with a crystallinity change during the burning process[32,53]. Interestingly, this effect was not identical for both types of bone presently investigated (femur and humerus), as reported for previous measurements on burned human bone[36], being more significant for femur regarding the OH signals (Fig. 6). This observation seems to imply that the effect of burning does not completely obliterate the differences in the skeletal samples prior to burning and needs further investigation. The signals undergoing defined wavenumber deviations upon burning may be taken as reliable biomarkers (proxies) of heat-prompted microcrystallinity rearrangements (Table 2). Their unequivocal assignment and relationship to FTIR-ATR data – quite straightforward for these infrared active $OH_{lib}$, $OH_{stretch}$ and $\nu_4(PO_4^{3-})$ bands – will enable a routine analysis of burned bone samples through this easy-to-use, benchtop vibrational technique.

Figure 7 represents the whole vibrational profile of human femur burned at 1000 °C, obtained by FTIR-ATR, Raman and INS (measured in both MAPS and TOSCA), as an example of the complementary information only accessible for these types of samples through the combined use of several vibrational techniques. While the $\nu_3^{as}(PO_4^{3-})$ and $\nu_3(CO_3^{2-})_{B/A}$ modes are clearly detected in the infrared, Raman allows us to observe $\nu_1(PO_4^{3-})$, $\nu_4(PO_4^{3-})$, $\nu_2(PO_4^{3-})$ and $\nu_1(CO_3^{2-})_B$, and INS yields the low frequency lattice modes of bone's inorganic matrix as well as hydroxyapatite's OH libration and stretching (detected simultaneously with very high sensitivity).

Throughout the burning process, the most significant spectral differences were observed between 700 and 800 °C and summarized in Fig. 8: (i) complete loss of the protein constituents (disappearance of amide I and II infrared bands, Fig. 2); (ii) significant narrowing of hydroxyapatite's $OH_{lib}$ and $\upsilon$(OH) INS signals (Figs 4 and 5(A)), and appearance of the $OH_{lib}$ infrared (Fig. 2); (iii) more defined lattice modes from the inorganic matrix, detected in far-IR and INS – namely (Ca–$PO_4$), $OH_{translation}$, and $\nu_2(HPO_4^{2-})/\nu_2(PO_4^{3-})$ (Figs 2 and 5(B)); (iv) appearance of the $\nu_3$(Ca–OH) INS feature (upon loss of type A carbonates) (Fig. 5(B)).

## Conclusions

The combined INS, Raman and infrared results presented here have enabled a thorough interpretation and validation of the existing vibrational spectroscopy data for skeletal human remains (including FTIR-derived indexes). Inelastic neutron scattering spectroscopy, in particular, led to the clarification of some unsettled issues such as: (i) the low energy vibrational pattern of bone subject to different temperatures; (ii) the temperature dependence

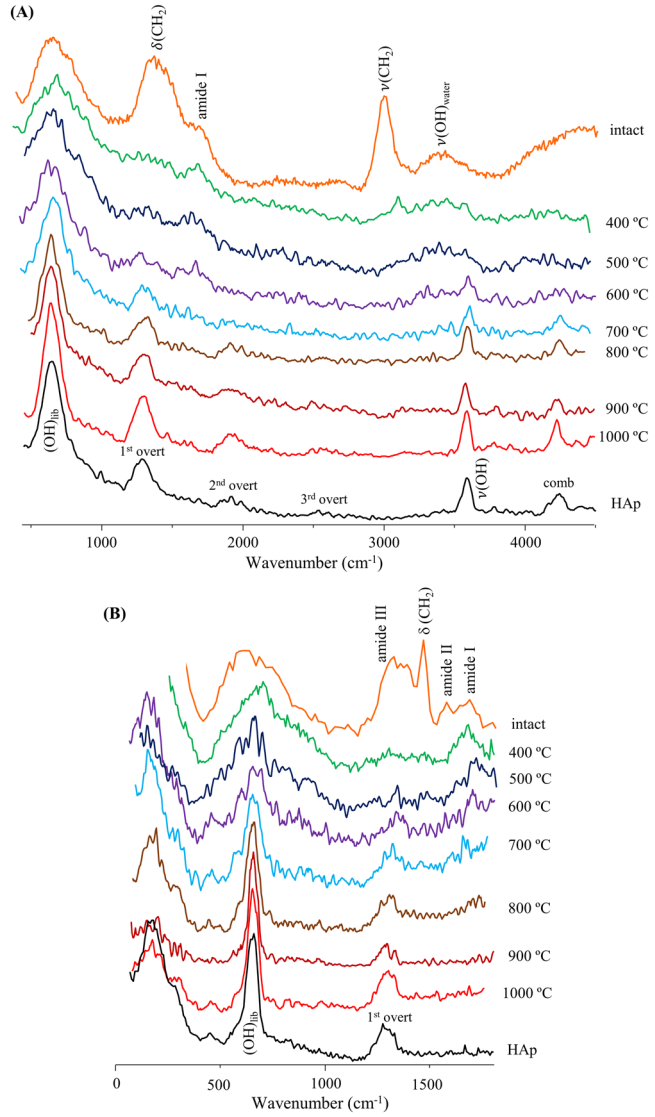


**Figure 4.** INS spectra, measured in MAPS, of human humerus: intact and burned at different temperatures (400 to 1000 °C). The spectra were recorded with 5240 (**A**) and 2024 $cm^{-1}$ (**B**) incident energies. The spectrum of reference calcium hydroxyapatite (HAp, SRM 2910b) is also shown for comparison.

of some characteristic lattice vibrational modes, and its relationship to hydroxyapatite's crystallinity; (iii) the presence of $HPO_4^{2-}$; (iv) the state of hydroxylation of bone's inorganic lattice; (v) the carbonate by hydroxyl substitution within bioapatite's matrix upon increasing temperatures (associated to the crystallite size). In addition, the combined MAPS and TOSCA experiments yielded a consistent set of results that were crucial for attaining an accurate assignment of the FTIR and Raman spectra (measured for the same samples), leading to the identification of reliable biomarkers (proxies) of heat-elicited diagenesis, namely $OH_{lib}$, $\nu$(OH) and $\nu_4(PO_4^{3-})$ bands, for which a distinctive quantitative temperature dependence was obtained.

This validates the analysis of burned skeletal remains by benchtop vibrational techniques such as FTIR-ATR, which is a low-cost, non-destructive and rapid method requiring very small amounts of bone and no sample preparation. The spectroscopic biomarkers of bone heat-induced diagenesis will be linked to pre-burned bone dimensions, finally providing a definitive correlation between crystalline structure and heat-prompted macroscopic dimensional changes. This should have an immediate impact on bone analysis, establishing FTIR-ATR as a routine technique for characterizing and identifying burned skeletal remains.

The innovative methodology reported presently as a way of understanding human bone tissue subject to high temperatures is expected to pave the way for the study of other types of skeletal materials (*e.g.* charred bone and teeth), leading to an improved understanding of heat-induced diagenetic processes. Such a quantitative method for assessing dimensional changes in burned human bones will be of the utmost significance in forensic, anthropological and archaeological sciences, namely for the analysis of burned bones found in crime scenes (*e.g.* victim identification) or in archaeological settings.

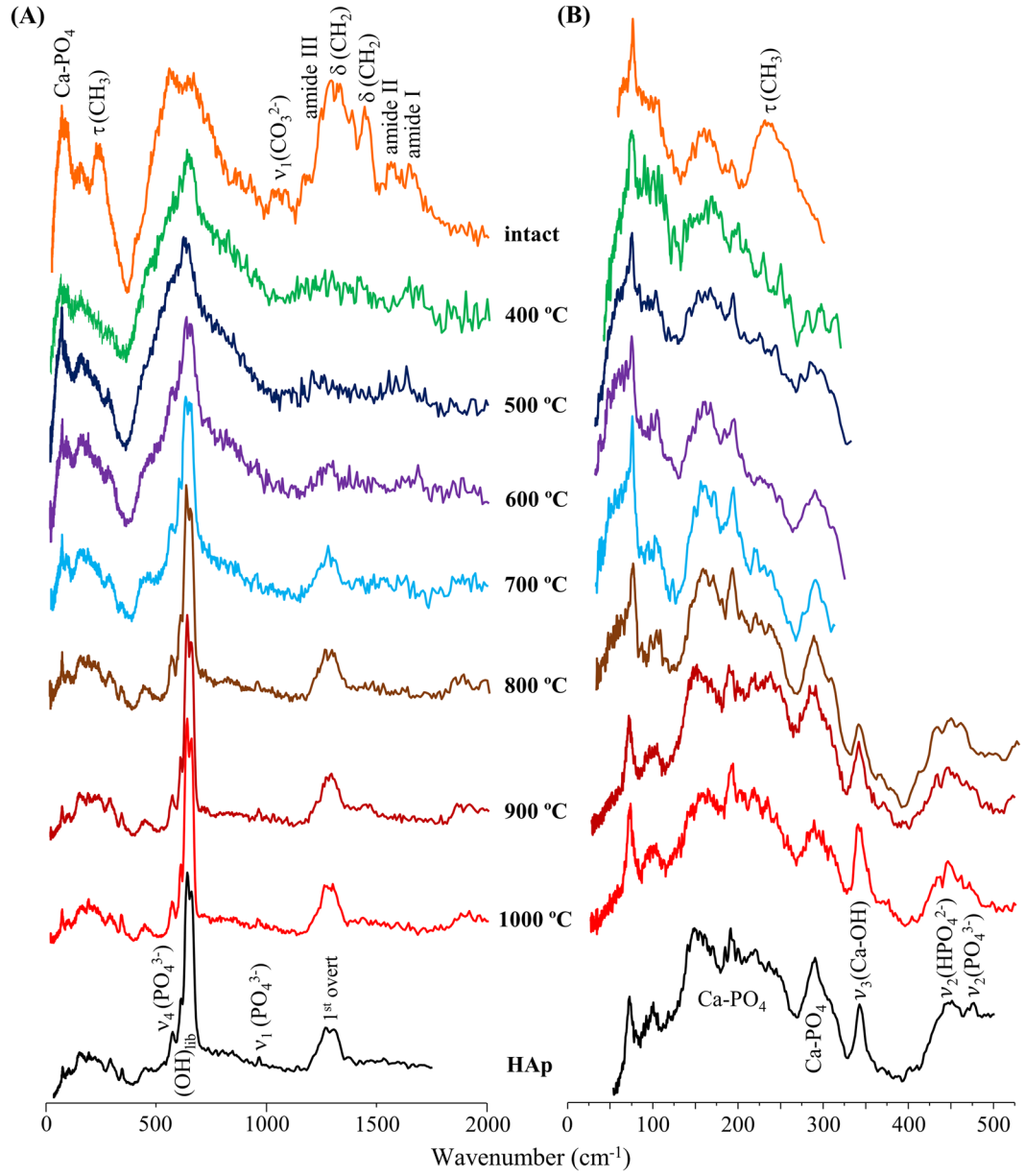


**Figure 5.** INS spectra, measured in TOSCA, of human femur: intact and burned at different temperatures (400 to 1000 °C). (**A**) 0 to 2000 $cm^{-1}$; (**B**) 0 to 550 $cm^{-1}$ (this region is expanded vertically for clarity sake). The spectrum of reference calcium hydroxyapatite (HAp, SRM 2910b) is also shown for comparison.

| Vibrational band | wavenumber ($cm^{-1}$) | detected by | heat-prompted variation |
|---|---|---|---|
| $\nu_3$(Ca–OH) | 330 | FTIR, INS | intensity decrease not detected <700 °C |
| $\nu_4(PO_4^{3-})$ | 574–617 | FTIR, INS | shift to higher frequency (600–1000 °C) not detected <600 °C |
| $(OH)_{lib}$ | 650 | FTIR, INS | shift to lower frequency |
| $\nu$(OH) | 3570 | FTIR, Raman, INS | shift to higher frequency |

**Table 2.** Vibrational biomarkers of heat-induced diagenesis in human bone.

## Materials and Methods

**Chemicals and Materials.** The bone samples, from the Laboratory of Forensic Anthropology of the University of Coimbra, were collected from an unidentified human skeleton from the cemetery of Capuchos (Santarém, Portugal)[54]. The exact inhumation period of this skeleton is unknown, but was at least 3 years. The current study was focused on two types of bones – femur and humerus – from the same skeleton, to avoid inter-skeleton variability[11]. These bones were already defleshed, *i.e.* completely devoid of both soft tissue and marrow.

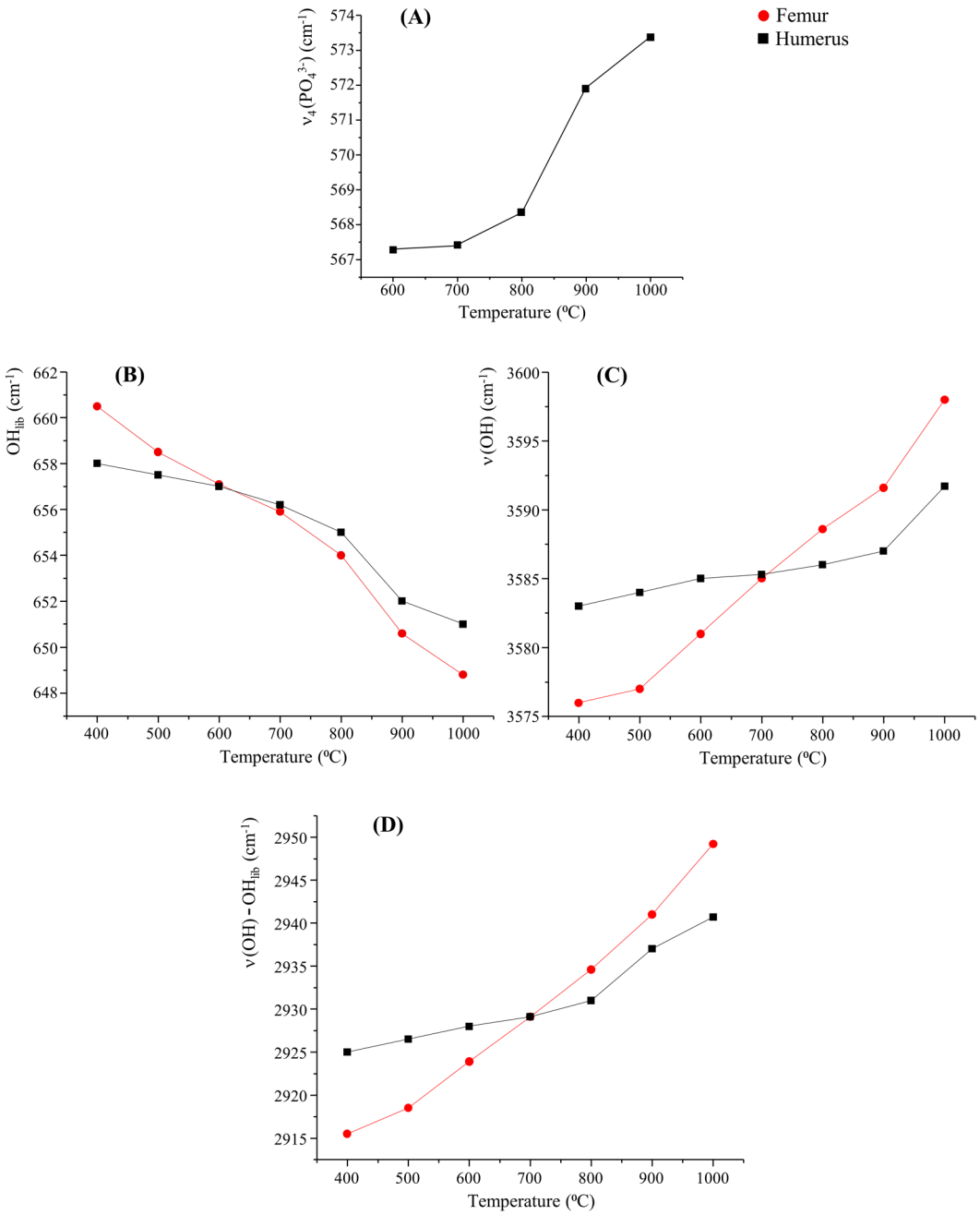


**Figure 6.** Temperature dependence of INS vibrational wavenumbers measured for human femur and humerus burned at different temperatures (400 to 1000 °C): (**A**) $\nu_4(PO_4^{3-})$; (**B**) $(OH)_{lib}$; (**C**) ν(OH); (**D**) ν(OH)-$(OH)_{lib}$.

Apart from the burned samples, data was also acquired for the same bones prior to burning (intact samples, ground), for comparison purposes. The sample preparation and controlled burning (400 to 1000 °C) are described in the Supporting Information. The highly crystalline sample of calcium hydroxyapatite ($Ca_2(PO_4)_6(OH)_2$, Ca/P = 1.67) from NIST (Gaithersburg, MA, USA)[55] was used as a reference (crystallinity index = 7.91, as compared to 3.79 for poorly crystalline commercial HAp).

*Sample Preparation and Controlled Bone Burning.* Femoral and humeral diaphyses were analysed (Fig. S1). After cutting each bone section (with a Dremel mini-saw electric tool), contaminants from the outer layer were removed by gentle sanding. For infrared and INS analysis, no further cleaning was needed[32]. Extensive handling was avoided, processes such as dehydration, defatting and deproteination being unnecessary for burned bones. Several adjacent bone slices were cut for each type of bone.

These bone fragments were subject to burning in an electric oven (Barracha K-3 three-phased 14 A), under controlled laboratory conditions regarding the intensity and duration of burning: temperatures in the range 400

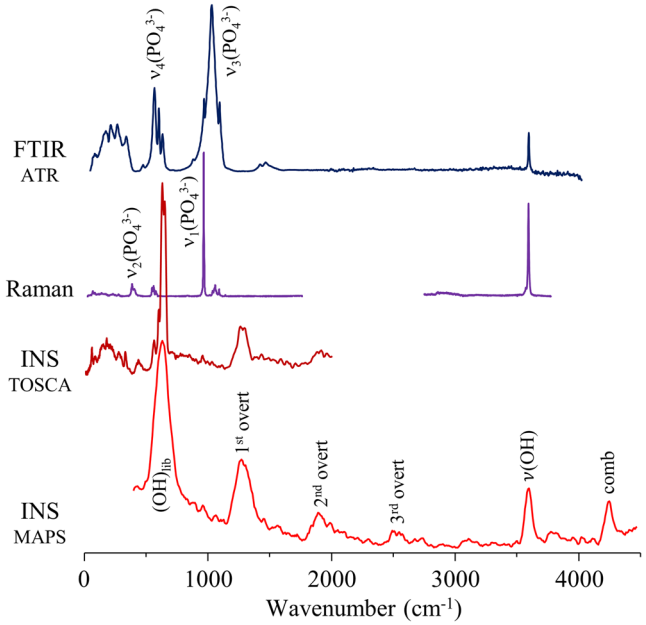


**Figure 7.** Vibrational profile – FTIR-ATR, Raman and INS (measured in TOSCA and MAPS) – of human femur burned at 1000 °C.

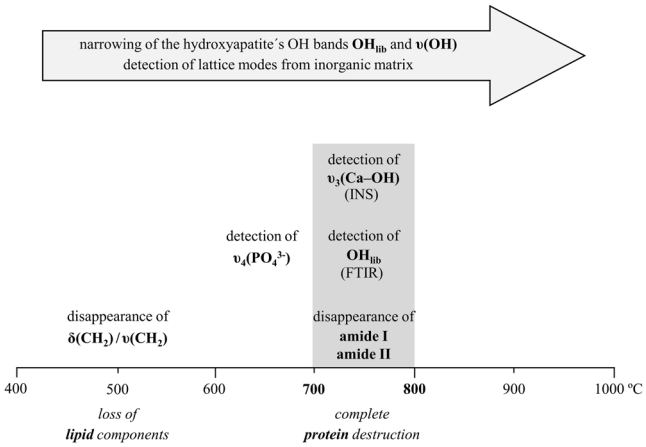


**Figure 8.** Schematic representation of the main spectral changes observed upon bone combustion (from 400 to 1000 °C).

to 1000 °C, at a heating rate *ca*. 6–10 °C/min, for 120 min. The burning process was performed in aerobic conditions (combustion). After burning, the bones were ground, followed by sieving (mesh size of 400 μm), yielding *ca*. 10 g of each sample.

Apart from the burned samples, data was also acquired for the same bones prior to burning (intact samples, ground), for comparison purposes.

**Fourier Transform Infrared Spectroscopy.** The FTIR-ATR spectra were acquired for the powdered bone samples using Bruker Optics Vertex 70 FTIR spectrometers purged by $CO_2$-free dry air and Bruker Platinum ATR single reflection diamond accessories. In the QFM-UC laboratory, a Ge on KBr substrate beamsplitter with a liquid nitrogen-cooled wide band mercury cadmium telluride (MCT) detector for the mid-IR interval (400–4000 $cm^{-1}$), and a Si beamsplitter with a room temperature deuterated L-alanine doped triglycine sulfate (DLaTGS) detector with a polyethylene window for the far-IR range (50–600 $cm^{-1}$), were used. At the ISIS Facility, a wide range MIR-FIR beamsplitter and a room temperature DLaTGS wide range detector were used (50–4000 $cm^{-1}$).

Each spectrum was the sum of 128 scans, at 2 $cm^{-1}$ resolution, and the 3-term Blackman–Harris apodization function was applied. Under these conditions, the wavenumber accuracy was better than 1 $cm^{-1}$. The spectra were corrected for the frequency dependence of the penetration depth of the electric field in ATR (considering a mean reflection index of 1.25) using the Opus 7.2 spectroscopy software.

**Raman Spectroscopy.** Raman spectra of the powdered bone samples (in the 100–1800 $cm^{-1}$ and 2750–3500 $cm^{-1}$ intervals) were recorded using a Horiba Jobin-Yvon T64000 spectrometer in direct configuration mode (focal distance 0.640 m, aperture f/7.5), equipped with a holographic grating of 1800 grooves·$mm^{-1}$. The entrance slit was set to 200 μm. Rayleigh elastic scattering was rejected by a notch filter, which reduces its intensity by a factor of $10^6$. The detection system was a liquid nitrogen cooled non-intensified 1024 × 256 pixels (1") CCD camera. The 514.5 nm line of an $Ar^+$ laser (Coherent, model Innova 300-05) was used as the excitation radiation, yielding ca. 10 mW at the sample position. All the spectra were recorded using an Olympus 50x objective (MSPlan 50, infinity corrected, NA 0.80, WD 0.47 mm).

All spectra were recorded with 5 accumulations and 30 seconds of exposure, at $<1$ $cm^{-1}$ spectral resolution, at room temperature with the samples placed onto glass microscope slides.

**Inelastic Neutron Scattering Spectroscopy.** The INS spectra were obtained at the ISIS Pulsed Neutron and Muon Source of the STFC Rutherford Appleton Laboratory (United Kingdom), using the time-of-flight, high resolution broad range spectrometers MAPS[56,57] and TOSCA[57–59].

In MAPS, three incident energies were used (968, 2024 and 5240 $cm^{-1}$) in order to accurately observe all the bands from bioapatite, in both the low and high frequency ranges – namely the OH libration, its overtones and the OH stretch mode.

The samples (4–10 g) were wrapped in aluminium foil and fixed onto 4 × 4 cm thin walled aluminium cans. To reduce the impact of the Debye-Waller factor (the exponential term in Equation (1)) on the observed spectral intensity, the samples were cooled to 5–10 K. Data were recorded in the energy range 0 to 6000 $cm^{-1}$ (MAPS) and 0 to 4000 $cm^{-1}$ (TOSCA), and converted to the conventional scattering law, $S(Q, \nu)$ *vs* energy transfer (in $cm^{-1}$) using the MANTID program (version 3.4.0)[60].

## Data Availability

The datasets generated during and/or analysed during the current study are available from the corresponding author upon reasonable request.

## References


1. Peters, F., Schwarz, K. & Epple, M. The structure of bone studied with synchrotron X-ray diffraction, X-ray absorption spectroscopy and thermal analysis. *Thermochim. Acta* **361**(1–2), 131–138 (2000).
2. Wang, X. Y., Zuo, Y., Huang, D., Hou, X. D. & Li, Y. B. Comparative study on inorganic composition and crystallographic properties of cortical and cancellous bone. *Biomed Environ Sci* **23**(6), 473–480 (2010).
3. Stathopoulou, E. T., Psycharis, V., Chryssikos, G. D., Gionis, V. & Theodorou, G. Bone diagenesis: New data from infrared spectroscopy and X-ray diffraction. *Palaeogeogr Palaeoclimatol Palaeoecol* **266**(3–4), 168–174 (2008).
4. Thompson, T. J. U., Gauthier, M. & Islam, M. The application of a new method of Fourier Transform Infrared Spectroscopy to the analysis of burned bone. *J Archaeol Sci* **36**(3), 910–914 (2009).
5. Thompson, T. J. U., Islam, M., Piduru, K. & Marcel, A. An investigation into the internal and external variables acting on crystallinity index using Fourier Transform Infrared Spectroscopy on unaltered and burned bone. *Palaeogeogr Palaeoclimatol Palaeoecol* **299**(1–2), 168–174 (2011).
6. King, C. L., Tayles, N. & Gordon, K. C. Re-examining the chemical evaluation of diagenesis in human bone apatite. *J Archaeol Sci* **38**(9), 2222–2230 (2011).
7. Hollund, H. I., Ariese, F., Fernandes, R., Jans, M. M. E. & Kars, H. Testing an alternative high-throughput tool for investigating bone diagenesis: Ftir in attenuated total reflection (atr) mode. *Archaeometry* **55**(3), 507–532 (2013).
8. Beasley, M. M., Bartelink, E. J., Taylor, L. & Miller, R. M. Comparison of transmission FTIR, ATR, and DRIFT spectra: Implications for assessment of bone bioapatite diagenesis. *J Archaeol Sci* **46**(1), 16–22 (2014).
9. Vassalo, A. R., Cunha, E., Batista de Carvalho, L. A. E. & Gonçalves, D. Rather yield than break: assessing the influence of human bone collagen content on heat-induced warping through vibrational spectroscopy. *Int J Legal Med* **130**(6), 1647–1656 (2016).
10. Mamede., A. P., Gonçalves, D., Marques, M. P. M. & Batista de Carvalho, L. A. E. Burned bones tell their own stories: A review of methodological approaches to assess heat-induced diagenesis. *Appl Spectrosc Rev* **53**(8), 603–635 (2018).
11. Gonçalves, D. *et al.* Crystal clear: Vibrational spectroscopy reveals intrabone, intraskeleton, and interskeleton variation in human bones. *Am J Phys Anthropol* **166**(2), 296–312 (2018).
12. Thompson, T. J. U. Recent advances in the study of burned bone and their implications for forensic anthropology. *Forensic Sci Int* **146**, S203–S205 (2004).
13. Thompson, T. J. U. Heat-induced dimensional changes in bone and their consequences for forensic anthropology. *J Forensic Sci* **50**, 185–193 (2005).
14. Symes, S. A., Rainwater, C. W., Chapman, E. N., Gipson, D. R. & Piper, A. L. Patterned Thermal Destruction ofHuman Remains in a Forensic Setting. *The Analysis ofBurned Human Remains*, eds Schmidt, C, Symes, S (Elsevier Ltd.), pp 15–50 (2008).
15. Ubelaker, D. H. The forensic evaluation of burned skeletal remains: A synthesis. *Forensic Sci Int* **183**(1–3), 1–5 (2009).
16. Vassalo, A. R., Mamede, A. P., Ferreira, M. T., Cunha, E. & Gonçalves, D. The G-force awakens: the influence of gravity in bone heat-induced warping and its implications for the estimation of the pre-burning condition of human remains. A*ust J Forensic Sci*. https://doi.org/10.1080/00450618.2017.1340521 (2017).
17. Cascant, M. M. *et al.* Burned bones forensic investigations employing near infrared spectroscopy. *Vib Spectrosc* **90**, 21–30 (2017).
18. Buckley, K., Matousek, P., Parker, A. W. & Goodship, A. E. Raman spectroscopy reveals differences in collagen secondary structure which relate to the levels of mineralisation in bones that have evolved for different functions. *J Raman Spectrosc* **43**(9), 1237–1243 (2012).
19. Sowoidnich, K. *et al.* Spatially offset Raman spectroscopy for photon migration studies in bones with different mineralization levels. *Analyst* **142**, 3219–3226 (2017).
20. Bachman, C. H. & Ellis, E. H. Fluorescence of Bone. *Nature* **206**, 1328–1331 (1965).
21. Wright, L. E. & Schwarcz, H. P. Infrared and Isotopic Evidence for Diagenesis of Bone Apatite at Dos Pilas, Guatemala: Palaeodietary Implications. *J Archaeol Sci* **23**(6), 933–944 (1996).
22. Trueman, C. N. G., Behrensmeyer, A. K., Tuross, N. & Weiner, S. Mineralogical and compositional changes in bones exposed on soil surfaces in Amboseli National Park, Kenya: Diagenetic mechanisms and the role of sediment pore fluids. *J Archaeol Sci* **31**(8), 721–739 (2004).
23. Lachowicz, J. I. *et al.* Multi analytical technique study of human bones from an archaeological discovery. *J Trace Elem Med Biol* **40**, 54–60 (2017).

24. Snoeck, C., Lee-Thorp, J. A. & Schulting, R. J. From bone to ash: Compositional and structural changes in burned modern and archaeological bone. *Palaeogeogr Palaeoclimatol Palaeoecol* **416**, 55–68 (2014).
25. Patonai, Z. *et al*. Novel dating method to distinguish between forensic and archeological human skeletal remains by bone mineralization indexes. *Int. J. Legal Med.* **127**(2), 529–533 (2013).
26. Mamede, A. P. *et al*. Potential of Bioapatite Hydroxyls for Research on Archeological Burned Bone. *Anal. Chem.* **90**(19), 11556–11563 (2018).
27. Howes, J. M., Stuart, B. H., Thomas, P. S., Raja, S. & O'Brien, C. An Investigation of Model Forensic Bone in Soil Environments Studied Using Infrared Spectroscopy. *J. Forensic Sci.* **57**, 1161–1167 (2012).
28. Longato, S. *et al*. Post-mortem interval estimation of human skeletal remains by micro-computed tomography, mid-infrared microscopic imaging and energy dispersive X-ray mapping. *Anal. Methods* **7**, 2917–2927 (2015).
29. Woess, C. *et al*. Assessing various Infrared (IR) microscopic imaging techniques for post-mortem interval evaluation of human skeletal remains. *PLoS One* **12**(3), e0174552 (2017).
30. Wang, Q. *et al*. Estimation of the late postmortem interval using FTIR spectroscopy and chemometrics in human skeletal remains. *Forensic Sci. Int.* **281**, 113–120 (2017).
31. Squires, K. E., Thompson, T. J. U., Islam, M. & Chamberlain, A. The application of histomorphometry and Fourier Transform Infrared Spectroscopy to the analysis of early Anglo-Saxon burned bone. *J Archaeol Sci* **38**, 2399–2409 (2011).
32. Thompson, T. J. U., Islam, M. & Bonniere, M. A new statistical approach for determining the crystallinity of heat-altered bone mineral from FTIR spectra. *J Archaeol Sci* **40**(1), 416–422 (2013).
33. Ellingham, S. T. D., Thompson, T. J. U., Islam, M. & Taylor, G. Estimating temperature exposure of burnt bone - A methodological review. *Sci Justice* **55**(3), 181–188 (2015).
34. Piga, G. *et al*. A structural approach in the study of bones: fossil and burnt bones at nanosize scale. *Appl Phys A* **122**(12), art 1031 (2016).
35. Abdel-Maksoud, G. & El-Sayed, A. Analysis of archaeological bones from different sites in Egypt by a multiple techniques (XRD, EDX, FTIR). *Mediterr Archaeol Archaeom* **16**(2), 149–158 (2016).
36. Marques, M. P. M., Gonçalves, D., Amarante, A. I. C., Makhoul, C. & Parker, S. F. & Batista de Carvalho, L. A. E. Osteometrics in burned human skeletal remains by neutron and optical vibrational spectroscopy. *RSC Adv* **6**(73), 68638–68641 (2016).
37. Carden, A. & Morris, M. D. Application of vibrational spectroscopy to the study of mineralized tissues (review). *J Biomed Opt* **5**(3), 259–268 (2000).
38. Monnier, G. F. A review of infrared spectroscopy in microarchaeology: Methods, applications, and recent trends. *J Archaeol Sci Reports* **18**, 806–823 (2018).
39. Loong, C.-K. *et al*. Evidence of hydroxyl-ion deficiency in bone apatites: an inelastic neutron-scattering study. *Bone* **26**(6), 599–602 (2000).
40. Taylor, M. G., Parker, S. F., Simkiss, K. & Mitchell, P. C. H. Bone mineral: evidence for hydroxy groups by inelastic neutron scattering. *Phys Chem Chem Phys* **3**(8), 1514–1517 (2001).
41. Taylor, M. G., Parker, S. F. & Mitchell, P. C. H. A study by high energy transfer inelastic neutron scattering spectroscopy of the mineral fraction of ox femur bone. *J Mol Struct* **651–653**, 123–126 (2003).
42. Bradtmiller, B. & Buikstra, J. E. Effects of burning on human bone microstructure: A preliminary study. *J Forensic Sci* **29**(2), 535–540 (1984).
43. Ellingham, S. T. D., Thompson, T. J. U. & Islam, M. The Effect of Soft Tissue on Temperature Estimation from Burnt Bone Using Fourier Transform Infrared Spectroscopy. *J Forensic Sci* **61**(1), 153–159 (2016).
44. Chikhani, M., Wuhrer, R. & Green, H. Optimization of Sample Preparation processes of Bone Material for Raman Spectroscopy. J *Forensic Sci*. https://doi.org/10.1111/1556-4029.13782 (2018).
45. Mamede, A. P. *et al*. Biomaterials from Human Bone – Probing Organic Fraction Removal by Chemical and Enzimatic Methods. *RSC Adv* **8**, 27260–27267 (2018).
46. LeGeros, R. Z., Trautz, O. R., Klein, E. & LeGeros, J. P. Two types of carbonate substitution in the apatite structure. *Experientia* **25**(1), 5–7 (1969).
47. Rey, C., Collins, B., Goehl, T., Dickson, I. R. & Glimcher, M. J. The carbonate environment in bone mineral: A resolution-enhanced fourier transform infrared spectroscopy study. *Calcif Tissue Int* **45**(3), 157–164 (1989).
48. Mkukuma, L. D. *et al*. Effect of the Proportion of Organic Material in Bone on Thermal Decomposition of Bone Mineral: An Investigation of a Variety of Bones from Different Species Using Thermogravimetric Analysis coupled to Mass Spectrometry, High-Temperature X-ray Diffraction. *Calcif Tissue Int* **75**(4), 321–328 (2004).
49. Fleet, M. E. Infrared spectra of carbonate apatites: $\nu 2$ Region bands. *Biomaterials* **30**(8), 1473–1481 (2009).
50. Xu, B. & Poduska, K. M. Linking crystal structure with temperature-sensitive vibrational modes in calcium carbonate minerals. *Phys Chem Chem Phys* **16**(33), 17634–17639 (2014).
51. Middendorf, H. D., Hayward, R. L., Parker, S. F., Bradshaw, J. & Miller, A. Vibrational neutron spectroscopy of collagen and model polypeptides. *Biophys J* **69**(2), 660–673 (1995).
52. Farlay, D., Panczer, G., Rey, C., Delmas, P. D. & Boivin, G. Mineral maturity and crystallinity index are distinct characteristics of bone mineral. *J Bone Miner Metab* **28**(4), 433–445 (2010).
53. Sui, T. *et al*. *In situ* X-ray scattering evaluation of heat-induced ultrastructural changes in dental tissues and synthetic hydroxyapatite. *J R Soc Interface* **11**(95), art 20130928 (2014).
54. Ferreira, M. T. *et al*. A new forensic collection housed at the University of Coimbra, Portugal: The 21st century identified skeletal collection. *Forensic Sci Int* **245**, 202.e1–202.e5 (2014).
55. National Institute of Standards and Technology (NIST) Available at, http://1.usa.gov/1WcMIO2 [Accessed June 2, 2018].
56. ISIS Facility INS – MAPS, https://www.isis.stfc.ac.uk/Pages/maps.aspx [Accessed June 21, 2018].
57. Parker, S. F., Lennon, D. & Albers, P. W. Vibrational spectroscopy with neutrons: A review of new directions. *Appl Spectrosc* **65**(12), 1325–1341 (2011).
58. ISIS Facility INS - TOSCA. Available at, https://www.isis.stfc.ac.uk/Pages/tosca.aspx [Accessed June 21, 2018].
59. Parker, S. F. *et al*. Recent and future developments on TOSCA at ISIS. *J Phys.: Conf. Ser.* **554**, 012003 (2014).
60. Arnold, O. *et al*. Mantid—Data analysis and visualization package for neutron scattering and μ SR experiments. *Nucl Instrum Methods Phys Res A* **764**, 156–166 (2014).


## Acknowledgements

The authors thank financial support from the Portuguese Foundation for Science and Technology – UID/MULTI/00070/2013, PEst-OE/SADG/UI0283/2013, PTDC/IVC-ANT/1201/2014 (POCI-01-0145-FEDER-016766) and SFRH/BPD/84268/2012. The STFC Rutherford Appleton Laboratory is thanked for access to neutron beam facilities.

## Author Contributions

M.P.M., D.G., S.P. and L.A.E.B.d.C. designed the experiments, experimental instructions, interpreted the data and contributed to the revising of the manuscript. A.V. and C.M. perform the bone controlled burn. M.P.M., A.M., A.V., C.M., D.G., S.P. and L.A.E.B.d.C. carried out the experiments and analysed the data. E.C. made the bone collection to perform the experiments available. M.P.M. wrote the manuscript and A.M. prepared the figures. All authors read and approved the final manuscript.

## Additional Information

**Supplementary information** accompanies this paper at https://doi.org/10.1038/s41598-018-34376-w.

**Competing Interests:** The authors declare no competing interests.

**Publisher's note:** Springer Nature remains neutral with regard to jurisdictional claims in published maps and institutional affiliations.

**Open Access** This article is licensed under a Creative Commons Attribution 4.0 International License, which permits use, sharing, adaptation, distribution and reproduction in any medium or format, as long as you give appropriate credit to the original author(s) and the source, provide a link to the Creative Commons license, and indicate if changes were made. The images or other third party material in this article are included in the article's Creative Commons license, unless indicated otherwise in a credit line to the material. If material is not included in the article's Creative Commons license and your intended use is not permitted by statutory regulation or exceeds the permitted use, you will need to obtain permission directly from the copyright holder. To view a copy of this license, visit http://creativecommons.org/licenses/by/4.0/.

© The Author(s) 2018